Open Ceramics 4 (2020) 100040

Contents lists available at ScienceDirect

Open Ceramics

journal homepage: www.editorialmanager.com/oceram

First time additively manufactured advanced ceramics by using two-photon polymerization for powder processing

Johanna C. Sänger *, Brian R. Pauw, Heinz Sturm, Jens Günster

Bundesanstalt für Materialforschung und -prüfung, Unter den Eichen 87, 12205, Berlin, Germany

ARTICLE INFO

Keywords:
Two photon polymerization
Alumina toughened zirconia
Additive manufacturing

ABSTRACT

Methods and materials: are presented here, which enable the manufacturing of fine structures using a 3D-printing method known as two-photon-polymerization (2PP). As traditional photolithography methods for structuring ceramic slurries do not function with 2PP, due to light scattering on ceramic particles, a novel water-based photoresist with high ceramic loading of extremely well dispersed ceramic nano particles was developed. This photoresist is basically a ceramic slurry containing a photocurable agent and a photoinitiator to be crosslinkable with the 780 nm wavelength femtosecond laser light source of the 2PP machine. It is demonstrated that it is possible to gain a highly transparent and low viscous slurry suitable for 2PP processing. This work shows the development of the slurry, first printing results and the post-printing processes required to form three dimensional ceramic microstructures consisting of alumina toughened zirconia (ATZ).

1. Introduction

Ceramics possess unique chemical and mechanical properties, such as mechanical strength, thermal stability, hardness, chemical resistance and special electrical, optical, and magnetic properties. By exploiting these unique properties, a great variety of technical and medical applications can be addressed. These include structured piezoelectric ceramics for ultrasonic transducers [1], customized bone implants made from hydroxyapatite [2], or bioglass/-TCP scaffolds [3,4] with promising biocompatibility and bespoke mechanical strength. For joint implants with high strength purpose, Alumina Toughened Zirconia (ATZ) is a desired material, due to its biocompatibility and mechanical behavior [5]. In particular for these medical and microengineering uses, the ability to introduce fine structures in materials is sorely needed. Additive manufacturing (AM) methods uniquely enable the formation of complex-shaped (e.g. porous) architectures. Here, AM complements traditional manufacturing in that it opens up completely new fields of research and applications [6]. Lithography based additive manufacturing of ceramics has been reviewed by Doreau et al. [7], with stereolithography methods standing out in particular, due to their high precision and fast production speeds. These methods can be either single beam processes or multi-beam/dynamic mask technologies [8–10]. The resolution of those processes can be optimized down to 10 μm in the XY-plane [11]. The Z-resolution is dependent on the technology shaping the single layers and rather higher than the XY-resolution, down to 2 μm [11]. Due to constraints imposed by the laws of physics, these lower resolution limits can only be further improved by exploiting nonlinear optical properties, as is done in two-photon polymerization (2PP). This technology can be applied to cross-link a range of polymer materials [12], printing ultrafine structures using the non-linear two-photon effect to confine the polymerizing voxel in three dimensions. However, producing 3D-structured ceramic parts using 2PP requires a careful design of the printing resin. A photocurable ceramic resin suitable for 2PP must meet a number of requirements, including a high transparency and a low viscosity, while maintaining a high ceramic content. Commercially available preceramic polymer options include Ormocer® [13] and SZ2080 [14] resins, which meet the aforementioned requirements [15]. With Ormocomp®, for example, a resolution can be achieved of 1 μm [16] or less [17], which is suitable for e.g. applications such as photonic crystals [18], microneedles [19], or even branched hollow fibers [20]. SZ2080 is a Zirconia-containing preceramic polymer, which can produce structures with tunable refractive index [21,22]. Moreover, tailored resins have been applied in combination with 2PP very successfully [23].

Compositing with particles can adjust the behavior of the final product. This has been demonstrated with piezoelectric barium titanate nanoparticles in Ormocomp® [24], Silica particles in polyvinylsilazane [25] or silica/gold nanoparticles [26].

Upon sintering, a ceramic is formed, which will mainly consist of

* Corresponding author.
E-mail addresses: johanna.saenger@bam.de (J.C. Sänger), jens.guenster@bam.de (J. Günster).

https://doi.org/10.1016/j.oceram.2020.100040
Received 29 October 2020; Received in revised form 24 November 2020; Accepted 30 November 2020
Available online 3 December 2020

silica/siliconoxicarbide SiOC [23,27]. To print full ceramic microstructures, another class of resin is needed, i.e. where the desired ceramic particles are embedded in a polymer filler that can be completely removed during sintering. The main challenge here is to fill the polymer with the highest possible weight fraction of ceramic particles, while maintaining the properties needed for the 2PP process. In this paper, the development of this new class of resin is introduced and first results of printed parts are presented.

2. Material and methods

The process chain from a ceramic-containing suspension (ceramic slurry) to a fully ceramic body follows the steps described in Fig. 1. A water-based suspension containing highly dispersed ceramic nanoparticles is also filled with the necessary photocuable agent and a suitable photoinitiator. This resin can be exposed to either UV-light or a 2PP-laser. Subsequently, the so called "green body" needs to be washed and dried, before it can be debinded to become a "brown body" and sintered. The sintering is the last and most important step to obtain ceramic bodies.

2.1. Material preperation and characterization

The nano-ceramic-additive-manufacturing (nanoCAM) photoresin was inspired by a slurry recipe for ceramic stereolithography [28] regarding the photocuable agent, i.e., Acrylamid and N,N′-methylene bisacrylamide. First a mixture of alumina oxide sol (Aerodisp W440, Evonik Industries AG) and zirconia oxide sol (Nanobinder NB 05, Nanostone Water Inc.) with a zirconia oxide/alumina oxide weight ratio of 80:20 has been dispersed in water to obtain a suspension with a total solid fraction of 65 wt%. After this, Acrylamid and N,N′-methylene bisacrylamide (Merck KGaA) is dissolved therein in a weight ratio of 10:1 to obtain photocurable properties in a resin with a ceramic load of 50 wt %, corresponding approximately 15,8 vol%. A photoinitiator suitable for the 2PP laser emitting at ca. 780 nm wavelength, consisting of 2,5-Bis [4-[N,N-Bis-[2-(Acetyloxy)Ethyl]Phenyl]-Methylene]-(2E,5E)-Cyclopentanone (BA740) [29], kindly provided by AG Schubert, Organic Chemistry II, University of Jena, is added at 1 wt % to trigger the desired photoreaction.

UV–vis measurements were performed using a StellarNet Inc. BLACK-Comet C-50 spectrometer with an SL5 deuterium + halogen light source. The samples were scanned in a cleavable quartz cell from Hellma Analytics with a thickness of 0,1 mm. The intensity-weighted mean size is determined using a Zetasizer (Nano ZS90, Malvern Pananalytica GmbH).

2.2. Two-photon-polymerization setup

Three-dimensional printing was performed using a Setup (Nanofactory, Femtika Ltd.) [24]. It incorporates a light source C-Fiber 780 High Power (Menlo Systems GmbH) operating at 100 fs pulse duration, 100 MHz repetition rate and 780 nm wavelength. The laser passes a 60 × 1.4 numerical aperture immersion oil objective lens (Carl Zeiss AG). The positioning system combines linear stages ANT130XY-160 (Aerotech Inc.) for XY-plane, ANT130LZS-060 (Aerotech Inc.), for Z direction, and galvo-scanners (AGV-10HPO (Aerotech Inc.) for image projection. Programming tasks and controlling the process where done by 3DPoli software (Femtika Ltd.).

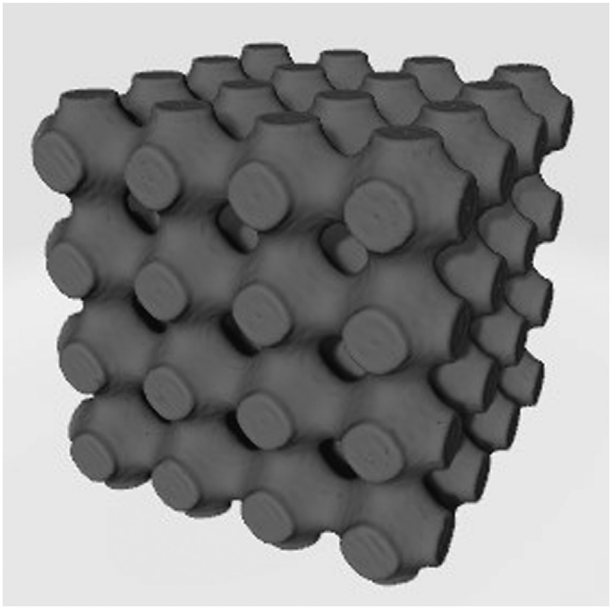

Fig. 2. Model of a half-filled SchwarzP-block consisting of 4 × 4 × 4 repeating unit cells.

2.3. Sample preparation, post-processing and characterization

An alumina plate is used as supporting substrate for the µm sized printed parts during printing, washing, debinding and sintering. On top of the supporting alumina plate 2–3 layers of a tape are glued to form a spacer of 100–200 µm, in which an area of a few millimeters is cut into, to form a process envelope. Inside this space, a drop of nanoCAM is placed, and subsequently covered by a thin microscopy cover glass with a thickness of 30 µm. On the supporting base a three-dimensional model of a SchwarzP triple periodic minimal surface [30] is printed. These SchwarzP cells are used as single repeating unit for generating scaffolds (see Fig. 2) with high mechanical strength, while minimizing the material consumption and the building time. With this particular SchwarzP-variation, one half space is filled to gain higher intrinsic strength during the writing process. This printable STL-file was produced using in-house developed software [34] based on an open source software [31].

Every structure is washed, using deionized water to remove uncured material, and dried after printing. Thermal debinding was performed between 325 and 375 °C and sintering at 1450 °C at a dwell of 100 min. The characterization of printed structures is performed using a scanning electron microscope (EVO MA10, Carl Zeiss GmbH) equipped with an energy dispersive X-ray detector from Thermo Fischer Scientific.

3. Results and discussion

3.1. Transparency

The optical properties of the suspensions used are extremely critical

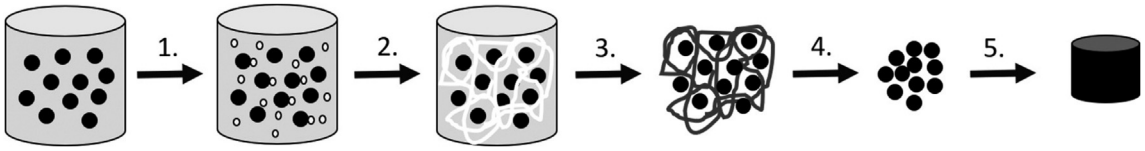

Fig. 1. Process chain beginning with water-based suspension with ceramic nanoparticles; 1. adding photocuring agent and photoinitiator to a slurry of well dispersed nano particles, 2. Photocuring, 3. washing and drying, 4. debinding, 5. Sintering.

to the process. Light is generally scattered by ceramic particles in water-based suspensions. On the other hand, light absorption is weak, as the pure ceramic material is a wide band gap insulator. The transparency of the ceramic suspensions, zirconia and alumina, was measured at 780 nm wavelength through different layer thicknesses to gain information about possible curing depths for the two-photon-setup. Two properties of the powders used are governing light scattering, the materials diffractive index and the particle size. To compare the two different powders, pure alumina and zirconia slurries have been prepared with near-identical ceramic content (50 wt % compared to 45 wt %, respectively). Fig. 3 is revealing the particle size distribution of the different slurries. It was found, that the larger particles of the alumina slurry scatter the light more effectively than the zirconia, even though zirconia has the higher refractive index of 2,1 than alumina of 1,7. This result is in accordance with the Rayleigh scattering regime [32], at which scattering is related to a decay in intensity I of $I \propto \lambda - 4$, as a function of the wavelength lambda.

For the final slurry, 80 wt % zirconia and 20 wt % alumina, a transmittance of 65% was measured at a penetration depth of 0,1 mm, which implies enough photons can pass through the nanoCAM photoresin to induce photopolymerization at the desired object size of maximal 100 µm.

3.2. 2PP production of ceramic parts

Before structures can be successfully printed, the operational parameter window (in particular the laser power, writing speed, and 2D hatching) must be defined. Due to intrinsic differences, this needs to be done for every material separately. For nanoCAM, this was done by printing one single SchwarzP unit cell in a 2D array whilst varying the laser power, writing steps (hatching distance) and scan speed from 500 μm/s to 4500 μm/s in 500 μm/s increments. As shown in Fig. 4, there exists a certain threshold at which the laser power is too low and the scan speed is too high for sufficient crosslinking. At a laser power output of lower than 12 mW the written structures completely collapse after washing and sintering. The clearest outline is visible in a powder range from 18 to 20 mW at a scan speed between 3500 and 4500 μm/s. This leads to an optimal setting at reasonable productivity of 4500 μm/s scan speed and 20 mW power output. It is noteworthy, that at a scan speed of 4500 μm/s, the laser spot distance between two adjacent laser pulses is in the range of 0.05 nm, bearing in mind that the laser is operated at a pulse repetition rate of 100 MHz.

The Stereo Lithography (STL) file is translated via a compiler into the machine code, providing the sliced object with a given thickness and hatch lines within one layer. If the hatching distance is too wide the structure will become unstable, and if it is too narrow, oversaturation results in distortions of printed object or even burning of the resin. Both parameters have been varied from 0,1 μm to 1,9 μm in steps of 0,2 μm. At a layer thickness of 0,3–0,5 μm and hatch distance of 0,3–0,7 μm the single units are the clearest. Also, at extreme parameter pairs with a maximum layer thickness of 1,9 μm and hatch distance of 0,1 μm and a minimum layer thickness of 0,1 μm with hatch distance of 1,9 μm good results are obtained. The latter parameters are useful for an increase of the process speed.

After compiling these findings, larger structures were configured, i.e. scaffolds comprised of 4 × 4 repeating unit cells (see Fig. 5), and subsequently fusing those scaffolds together to form 2 × 2 arrays of 100 × 100 μm. The operational parameters were a scan speed of 5000 μm/s, axis velocity of 1000 μm/s (for moving the objective in the stitching mode), laser output power of 20 mW, layer thickness of 0,99 μm and hatch distance of 0,1 μm. After washing, drying, debinding and sintering, a scaffold remains on the surface. Due to significant shrinkage of up to 50% during the post-processing, debinding and sintering in particular, the final shape is distorted, mostly in z-direction. A constrained sintering on the non-shrinking alumina substrate results in a distortion of the structure, most significantly along the z-axis. Nonetheless, Fig. 5 is a clear evidence, that 2PP processing of ceramic slurries is possible. Associated to Fig. 5 there is an additional learning: In the writing program, four SchwarzP 4 × 4 repeating unit cells were stitched together. That means each of the four 4 × 4 structures were written independently, by the imaging scanner optics without moving the objective. Stitching was achieved by a lateral movement of the objective relative to the substrate. This strategy is commonly applied to build up large structures with 2PP. However, the intrinsic stability is only given in structures that were written as a continuous structure without stitching. In the as-printed part the interface cannot be recognized, but after sintering. It is not exactly clear why these weak interfaces are formed, but very likely the ceramic particles are separated in an optical tweezer effect [33], drawing them into regions of highest laser intensity, which finally would result in an entirely polymeric interface leaving a ceramic material gap after sintering.

To address the distortion of the printed object occurring during shrinkage, one tiny scaffold was placed on a sacrificial support structure

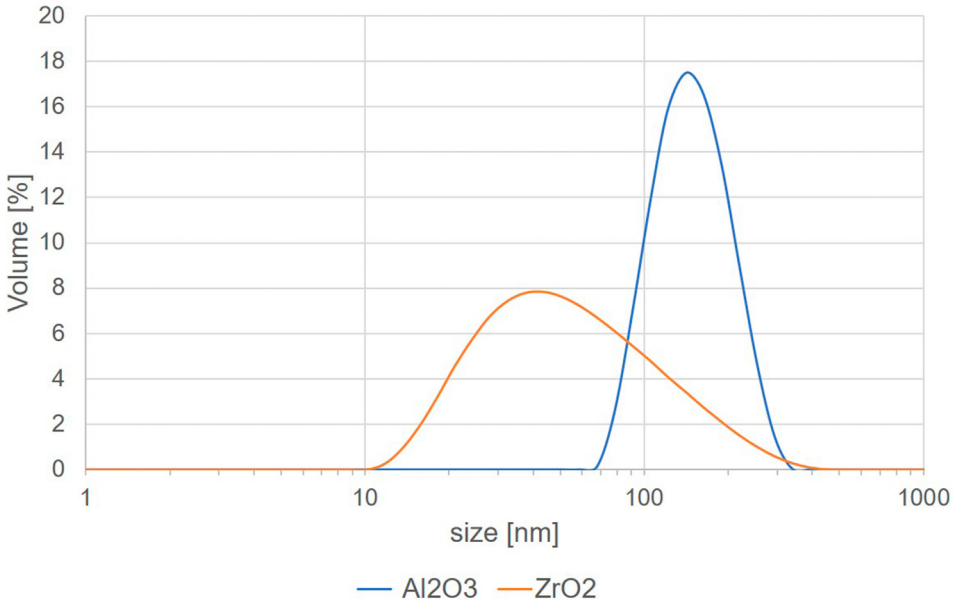

Fig. 3. Particle size distribution of zirconia alumina suspension.

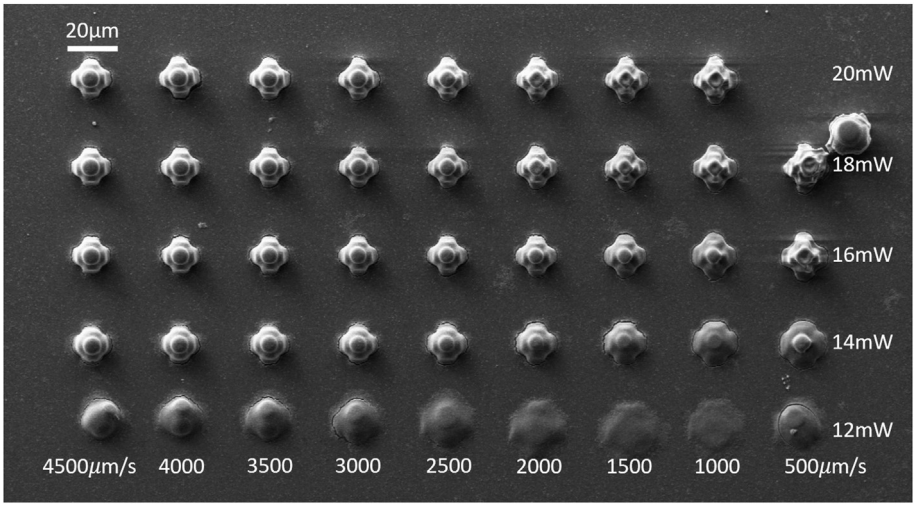

Fig. 4. Scan speed and laser power output map to find suitable writing parameters. For reducing the process time, the results shown are obtained at a relative high layer thickness of 0.99 µm and a hatch distance of 0.1 µm.

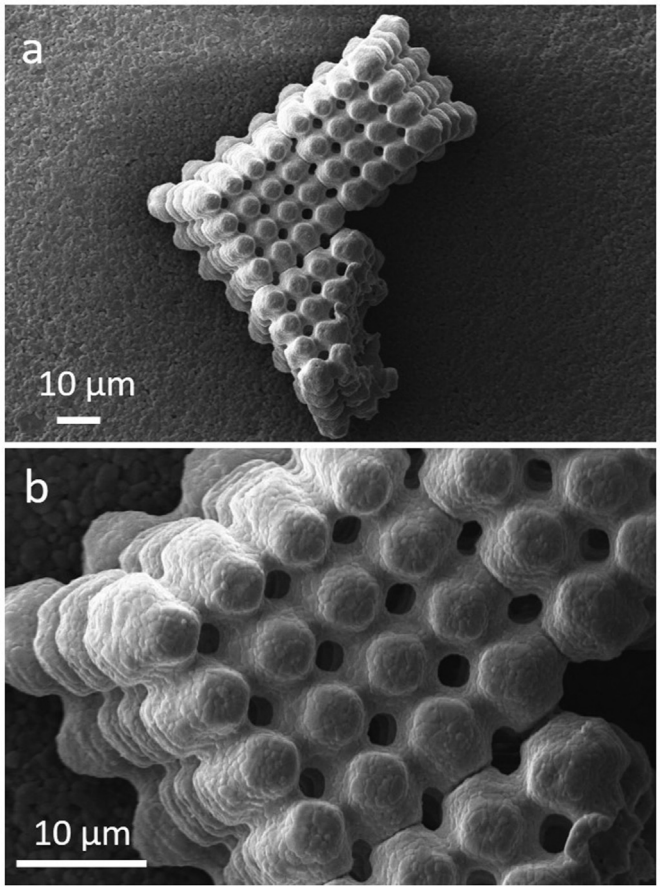

Fig. 5. SEM images of a 2PP-printed fully ceramic scaffold (a) one 4 × 4 SchwarzP unit with two adjacent 4 × 4 units, (b) detailed view.

comparable to the approach presented by Brigo et al. [23], which is, however, destroyed during the post-processing, see Fig. 6. Originally the support was a simple cylinder, which completely disintegrated due to internal stress into an irregular structure as shown. Nonetheless, it gave the scaffold the possibility to shrink uniformly and preserved its shape in all three dimensions.

The ceramic nature of the structures shown has been confirmed by

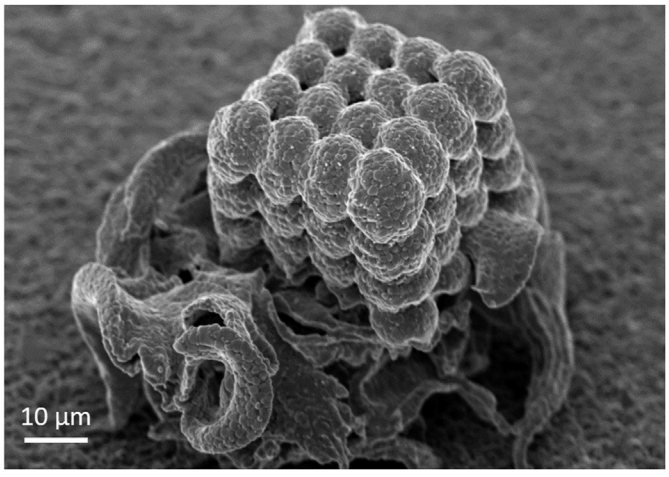

Fig. 6. Scaffold on top of a support structure completely disintegrated by the enormous stress associated to sintering shrinkage on the rigid, non-shrinking supporting alumina support.

Energy-dispersive X-ray spectroscopy (EDX), revealing the correct ratio between zirconium, aluminum and oxygen atoms required to form alumina toughened zirconia. In addition, an image taken from the structure by an SEM operated in electron back scatter mode clearly confirms that the structure is composed out of two species, one with heavier elements, i.e., zirconia (brighter structures in Fig. 7 a), and one with lighter elements, i.e. alumina (darker structures in Fig. 7a). The as-sintered surface shown does not exactly resemble the expected microstructure of 30 nm zirconia and 200 nm alumina particles. Apparently, due to the high sintering activity of the extremely well dispersed and closely packed zirconia nanoparticles, domains of densely sintered zirconia are formed. Also, it is not clear at which extend the scanning of the laser beam is influencing the particles micro structure, by the previously mentioned optical tweezer effect and local crosslinking of the polymer matrix. For the fist time, these effects need to be considered in ceramics powder processing.

4. Conclusion

This study demonstrates the smallest additively manufactured ceramic nanostructure using two photon polymerization. To achieve this,

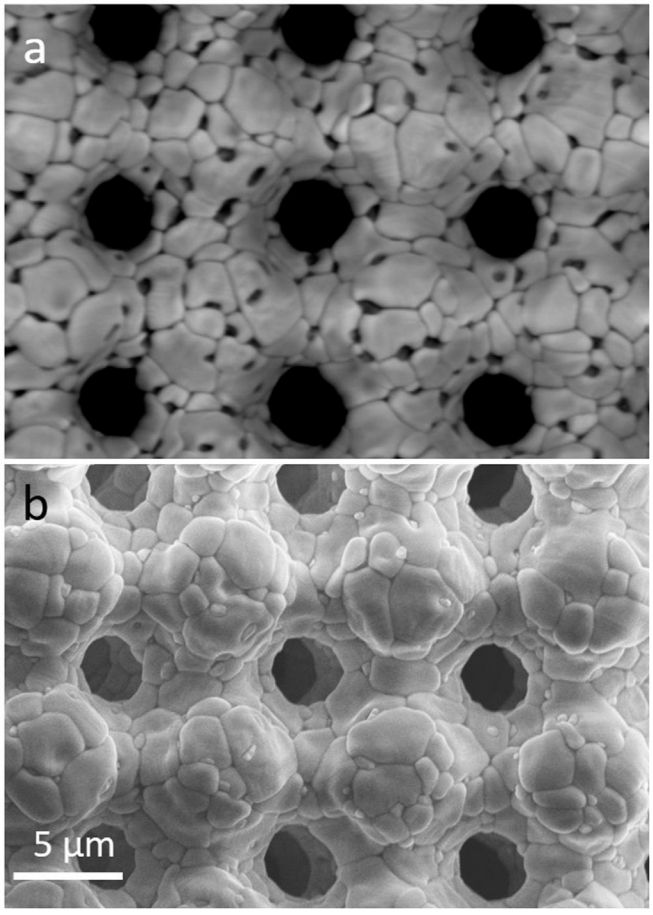

Fig. 7. (a) Electron back scatter image and (b) secondary electron image of a 2PP alumina toughened zirconia structure after sintering.

a resin, nanoCAM, has been developed, containing extremely well dispersed ceramic nanoparticles to overcome the light scattering-imposed limitations. The suspension meets the criteria for two photon polymerization, being viscous enough for processing, photocurable to build up mechanical strength and sufficiently transparent at the desired wavelength range. This result should encourage other groups to combine classical ceramic processing with two-photon polymerization (2PP) technology for the manufacture of smallest advanced ceramics structures and taking advantage of their superior physicochemical properties even.

Acknowledgements

We would like to express special thanks Herrn Christian Göbbert from Nanostone Water Inc. Providing us with ceramic-containing nano suspensions.

References

[1] M. Cheverton, P. Singh, L.S. Smith, K.P. Chan, J.A. Brewer, V. Venkataramani, Ceramic polymer additive manufacturing system for ultrasound transducer, Proceedings of solid freeform fabrication symposium (2012) 863–875.
[2] E. Cunningham, N. Dunne, G. Walker, F. Buchanan, High-solid-content hydroxyapatite slurry for the production of bone substitute scaffolds, J. of Engineering in Medicine 223 (2009) 727–737.
[3] W. Bian, D. Li, Q. Lian, X. Li, W. Zhang, K. Wang, Z. Jin, Fabrication of a bio-inspired beta-Tricalcium phosphate/collagen scaffold based on ceramic stereolithography and gel casting for osteochondral tissue engineering, Rapid Prototyp. J. 18 (2012) 68–80.
[4] R. Felzmann, S. Gruber, G. Mitteramskogler, P. Tesavibul, A.R. Boccaccini, R. Liska, J. Stampfl, Lithography-based additive manufacturing of cellular ceramic structures, Adv. Eng. Mater. 14 (2012) 1052–1058.
[5] E. Schwarzer, S. Holtzhausen, U. Scheithauer, C. Ortmann, T. Oberbach, T. Moritz, A. Michaelis, Process development for additive manufacturing of functionally graded alumina toughened zirconia components intended for medical implant application, J. Eur. Ceram. Soc. 39 (2019) 522–530.
[6] A. Zocca, P. Colombo, C.M. Gomes, J. Günster, Additive manufacturing of ceramics: issues, potentialities, and opportunities, J. Am. Ceram. Soc. 98 (2015) 1983–2001.
[7] F. Doreau, C. Chaput, T. Chartier, Stereolithography for manufacturing ceramic parts, Adv. Eng. Mater. 2 (2000) 493–496.
[8] R. Gmeiner, G. Mitteramskogler, J. Stampfl, A.R. Boccaccini, Stereolithographic ceramic manufacturing of high strength bioactive glass, Int. J. Appl. Ceram. Technol. 12 (2015) 38–45.
[9] J.W. Halloran, V. Tomeckova, S. Gentry, S. Das, P. Cilino, D. Yuan, R. Guo, A. Rudraraju, et al., Photopolymerization of powder suspensions for shaping ceramics, J. Eur. Ceram. Soc. 31 (2011) 2613–2619.
[10] M. Schwentenwein, P. Schneider, J. Homa, Lithography-based ceramic manufacturing: a novel technique for additive manufacturing of highperformance ceramics, Adv. Sci. Technol. 88 (2014) 60–64.
[11] S. Kirihara, N. Toshiki, Three-dimensional stereolithography of alumina photonic crystals for terahertz wave localization, Int. J. Appl. Ceram. Technol. 12 (2015) 32–37.
[12] C.N. LaFratta, J.T. Fourkas, T. Baldacchini, R.A. Farrer, Multiphoton fabrication, Angew. Chem. Int. Ed. 46 (2007) 6238–6258.
[13] K.-H. Haas, Hybrid inorganic–organic polymers based on organically modified Si-alkoxides, Adv. Eng. Mater. 2 (2000) 571–582.
[14] M. Farsari, B.N. Chichkov, Materials processing: two-photon fabrication, Nat. Photon. 3 (2009) 450.
[15] J. Serbin, A. Egbert, A. Ostendorf, B.N. Chichkov, R. Houbertz, G. Domann, J. Schulz, C. Cronauer, et al., Femtosecond laser-induced two-photon polymerization of inorganic–organic hybrid materials for applications in photonics, Opt. Lett. 28 (2003) 301–303.
[16] E. Käpylä, S. Turunen, J. Pelto, J. Viitanen, M. Kellomäki, Investigation of the optimal processing parameters for picosecond laser-induced microfabrication of a polymer–ceramic hybrid material, J. Micromech. Microeng. 21 (2011), 065033.
[17] M. Farsari, G. Filippidis, C. Fotakis, Fabrication of three-dimensional structures by three-photon polymerization, Opt. Lett. 30 (2005) 3180–3182.
[18] A. Ovsianikov, A. Ostendorf, B.N. Chichkov, Three-dimensional photofabrication with femtosecond lasers for applications in photonics and biomedicine, Appl. Surf. Sci. 253 (2007) 6599–6602.
[19] A. Ovsianikov, B. Chichkov, P. Mente, N.A. Monteiro-Riviere, A. Doraiswamy, R.J. Narayan, Two photon polymerization of polymer–ceramic hybrid materials for transdermal drug delivery, Int. J. Appl. Ceram. Technol. 4 (2007) 22–29.
[20] M. Bieda, F. Bouchard, A.F. Lasagni, Two-photon polymerization of a branched hollow fiber structure with predefined circular pores, J. Photochem. Photobiol. Chem. 319 (2016) 1–7.
[21] A. Ovsianikov, J. Viertl, B. Chichkov, M. Oubaha, B. MacCraith, I. Sakellari, A. Giakoumaki, D. Gray, et al., Ultra-low shrinkage hybrid photosensitive material for two-photon polymerization microfabrication, ACS Nano 2 (2008) 2257–2262.
[22] L. Jonušauskas, D. Gailevičius, L. Mikoliūnaitė, D. Sakalauskas, S. Šakirzanovas, S. Juodkazis, M. Malinauskas, Optically clear and resilient free-form μ-optics 3D-printed via ultrafast laser lithography, Materials 10 (2017) 12.
[23] L. Brigo, J.E.M. Schmidt, A. Gandin, N. Michieli, P.- Colombo, G. Brusatin, 3D nanofabrication of SiOC ceramic structures, Adv. Sci. (2018), 1800937.
[24] L. Jonušauskas, T. Baravykas, D. Andrijec, T. Gadišauskas, V. Purlys, Stitchless support-free 3D printing of free-form micromechanical structures with feature size on-demand, Sci. Rep. 9 (1) (2019) 1–12.
[25] T.A. Pham, D.-P. Kim, T.-W. Lim, S.-H. Park, D.-Y. Yang, K.-S. Lee, Threedimensional SiCN ceramic microstructures via nano-stereolithography of inorganic polymer photoresists, Adv. Funct. Mater. 16 (2006) 1235–1241.
[26] Y. Li, L. Chen, F. Kong, Z. Wang, M. Dao, C.T. Lim, F. Li, M. Hong, Functional micro-concrete 3D hybrid structures fabricated by two-photon polymerization, Opto-Electronic Eng. 44 (2017) 393–399.
[27] C.W. Ha, P. Prabhakaran, K.-S. Lee, Versatile applications of three-dimensional objects fabricated by two-photon-initiated polymerization, MRS Communications 9 (2019) 53–66.
[28] W. Bian, D. Li, Q. Lian, W. Zhang, L. Zhu, X. Li, Z. Jin, Design and fabrication of a novel porous implant with pre-set channels based on ceramic stereolithography for vascular implantation, Biofabrication 3 (2011), 034103.
[29] L. Poocza, M. Gottschaldt, E. Markweg, N. Hauptmann, G. Hildebrand, D. Pretzel, M. Hartlieb, C. Reichardt, et al., Optimized photoinitiator for fast two-photon absorption polymerization of polyester-macromers for tissue engineering, Adv. Eng. Mater. 19 (2017) 1600686.
[30] P.J.F. Gandy, J. Klinowski, Exact computation of the triply periodic Schwarz P minimal surface, Chem. Phys. Lett. 322 (2000) 579–586.
[31] J.C. Dinis, T.F. Morais, P.H.J. Amorim, R.B. Ruben, H.A. Almeida, P.N. Inforçati, P.J. Bártolo, J.V.L. Silva, Open source software for the automatic design of scaffold structures for tissue engineering applications, Procedia Technology 16 (2014) 1542–1547.
[32] C.E. Barnett, Some applications of wave-length turbidimetry in the infrared, J. Phys. Chem. 46 (1942) 69–75.
[33] D. Gao, W. Ding, M. Nieto-Vesperinas, X. Ding, M. Rahman, T. Zhang, C.-T. Lim, C.-W. Qiu, Optical manipulation from the microscale to the nanoscale: fundamentals, advances and prospects, Light Sci. Appl. 6 (2017) 17039.
[34] https://github.com/BAMresearch/ScaffoldStructures.